Optical modes of micropillar cavities

Keesjan de Vries

Bachelor Thesis
Leiden University
Leiden Institute of physics

August 18, 2009

Contents

Chapter 1

Abstract

In this thesis we investigate the optical modes of micropillar cavities. With our experimental setup it is possible to investigate their spatial structure. A simple model provides accurate predictions on the wavelength and the spatial structure of the modes.

Chapter 2

Introduction

2.1 Microcavities

In modern physics a great deal of research is performed on optical microcavities, which confine light to small volumes by resonant recirculation[1]. One of the ultimate applications would be to build a quantum computer using local (two-level) quantum systems in the cavities as qubits (unit of quantum information). Examples of these quantum systems are quantum dots or trapped atoms. Due to small dimensions, microcavities have well defined *discrete (optical) modes*. The coupling between these cavity modes and the local quantum system should form the basis for calculation methods of quantum computers.

2.2 Micropillar cavities

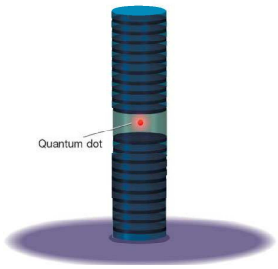

Figure 2.1: Example of a quantum dot in a micropillar cavity.

One type of local quantum systems in optical microcavities are quantum dot in micropillar cavities (see Fig. 2.2). The 'pillars' are etched in crystalline structures. They consist of an active λ-cavity region embedded between two distributed Bragg reflector(DBR). A distributed bragg reflector consists of $\lambda/4$-

layers of alternating refractive index, typically AlGaAs/GaAs. This way the DBR has a maximal reflection of light with wavelength λ. The λ-cavity region consists typically of GaAs and some additional layers.

2.2.1 Our cavities

The sample that will be studied in this thesis contains micropillar cavities with a quantum dot layer. The special features of these cavities are that they are etched by only removing some trenches (see Fig. 2.2.1) and that there is an *oxide aperture* grown between the two Bragg mirrors.

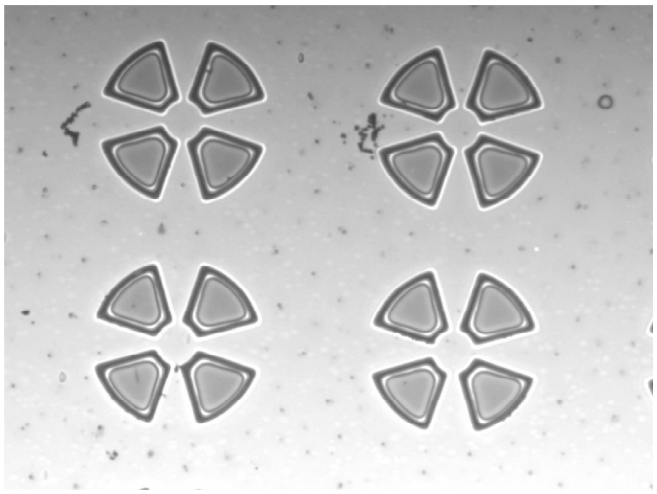

Figure 2.2: Microscope image of the sample. The micropillar are fabricated by etching away trenches from the wafer.

2.3 Aim of this thesis

The aim of this thesis is to find a good description of the optical modes within our cavities. If we have a good description, we may be able to tune these modes in order to get a good coupling with the quantum dots.

Chapter 3

Theoretical model

3.1 Simple model for the refractive index distribution

Let us see whether we can think of a theoretical model which provides us with predictions for the cavity modes. In the following we tightly follow the treatment of optical fibers in "QUANTUM ELECTRONICS" by Amnon Yariv (third edition, pages 640 and 641).

For finding optical modes within our cavities we have to solve the wave equation in material

$$\nabla^2 \mathbf{E}(\mathbf{r}) + k_0^2 n^2(\mathbf{r}) \mathbf{E}(\mathbf{r}) = 0, \tag{3.1}$$

with $\mathbf{E}$ the electric field, $k_0 = \omega/c$ the wave number in vacuum, and $n(\mathbf{r})$ the refractive index distribution. Note that this is the wave equation for an isotropic material. We assume that within the cavity the refractive index equals

$$n(\mathbf{r})^2 = n^2(x, y) = n_0^2 \left(1 - \frac{x^2}{r_x^2} - \frac{y^2}{r_y^2} \right). \tag{3.2}$$

Here x and y are taken perpendicular to the the z-axis through the center of the cavity. Note that we assume that the refractive index is constant in the vertical direction and quadratically decreasing in the x- and y- direction. This is one of the most simple ways to take into account that the oxide aperture will induce a refractive index which is smoothly (not perfectly symmetrically) decreasing when going away from the center. As we shall see this results in a nicely solvable problem. Substituting Eq. 3.2 into Eq. 3.1 yields

$$\nabla^2 \mathbf{E}(\mathbf{r}) + k^2 \left(1 - \frac{x^2}{r_x^2} - \frac{y^2}{r_y^2} \right) \mathbf{E}(\mathbf{r}) = 0, \tag{3.3}$$

with $k = k_0 n_0$. We will first consider some scalar some *scalar component* E of $\mathbf{E}$. We suggestively assume that

$$E(\mathbf{r}) = \psi(x, y) sin \left(\frac{l\pi}{h} z \right), \tag{3.4}$$

and write $\psi(x,y) = f(x)g(y)$. The choice for the z-part of Eq. 3.4 expresses the fact that we expect confinement in the z-direction, i.e. the wave function vanishes at the two Bragg mirrors, or rather within them. The places where $E(z)$ vanishes are separated by an effective height h. Note that the origin is taken at the bottom of the cavity. Furthermore $l = 1, 2, ...$ and indicates the mode number of the z-component. If we write

$$\beta_l = \frac{l\pi}{h}, \tag{3.5}$$

the wave equation Eq. 3.3 becomes

$$\frac{1}{f}\frac{\partial^2 f}{\partial x^2} + \frac{1}{g}\frac{\partial^2 g}{\partial y^2} - \beta_l^2 + k^2\left(1 - \frac{x^2}{r_x^2} - \frac{y^2}{r_y^2}\right) = 0, \tag{3.6}$$

which is the sum of respectively the x- and y-dependent equations

$$\frac{1}{f}\frac{d^2 f}{dx^2} + k^2 - \beta_l^2 - \frac{k^2 x^2}{r_x^2} = C \tag{3.7}$$

$$\frac{1}{g}\frac{d^2 g}{dy^2} - \frac{k^2 y^2}{r_y^2} = -C \tag{3.8}$$

with C some constant. We first consider Eq. 3.8. By introducing

$$\xi = \alpha_y y \quad \text{and} \quad \alpha_y \equiv \left(\frac{k}{r_y}\right)^{1/2}, \tag{3.9}$$

Eq. 3.7 becomes

$$\frac{d^2 g}{d\xi^2} + \left(\frac{C}{\alpha_y^2} - \xi^2\right) g = 0. \tag{3.10}$$

This is an equation we can solve, because it is the same as the Schrödinger equation for a harmonic oscillator [2]. We get for C/α_y^2

$$\frac{C}{\alpha_y^2} = 2m + 1, \tag{3.11}$$

where $m = 0, 1, 2, ...$ The corresponding eigenfunctions are

$$g_m(\xi) = H_m(\xi)e^{-\xi^2/2} \tag{3.12}$$

with $H_m(\xi)$ the Hermite polynomial of order m (see appendix A).

Now defining

$$\zeta = \alpha_x y \quad \text{and} \quad \alpha_x \equiv \left(\frac{k}{r_x}\right)^{1/2}, \tag{3.13}$$

Eq. 3.7 becomes

$$\frac{d^2 f}{d\zeta^2} + \left(\frac{k^2 - \beta_l^2 - C}{\alpha_s^2} - \xi^2\right) f = 0, \tag{3.14}$$

which gives

$$\frac{k^2 - \beta_l^2 - C}{\alpha_x^2} = 2n + 1, \tag{3.15}$$

with corresponding eigenfunctions

$$f_n(\zeta) = H_n(\zeta) e^{-\zeta^2/2}. \tag{3.16}$$

Putting together Eqs. 3.16 and 3.12 for $\psi(x, y)$ we get

$$\psi_{[nm]}(x, y) = H_n\left(\frac{\sqrt{2}x}{w_x}\right) H_m\left(\frac{\sqrt{2}y}{w_y}\right) e^{-\left(\frac{x^2}{w_x^2} + \frac{y^2}{w_y^2}\right)}, \tag{3.17}$$

where

$$w_{x,y} = \frac{\sqrt{2}}{\alpha_{x,y}} = \sqrt{\frac{2r_{x,y}}{k}} \tag{3.18}$$

corresponds to the "spot size". We call these functions *Hermite Gaussians*. Fig. 3.1 shows some examples of $\psi_{[nm]}$.

3.1.1 Spectrum of the modes

So far we solved wave equation Eq. 3.1 for a scalar part of $\mathbf{E}$, assuming confinement in the z-direction assuming and quadratically decreasing refractive index (Eq. 3.2). From this we obtained the eigenfunctions $E(\mathbf{r}) = \psi_{[nm]}(x, y) sin(\beta_l z)$, with $\psi_{[nm]}(x, y)$ as in equation 3.17 and β_l as in Eq. 3.5.

We will now have a look at the eigenvalues of the eigenfunctions and thereby the spectrum of the cavity. We need to solve k and thus λ for a certain combination of n and m. From Eqs. 3.15 and 3.11 we obtain

$$k^2 - \beta_l^2 - \alpha_y^2 (2m + 1) = \alpha_x^2 (2n + 1) \tag{3.19}$$

or

$$k^2 - 2\gamma k - \beta_l^2 = 0 \tag{3.20}$$

with $2\gamma = \left\{ \frac{(2n+1)}{r_x} + \frac{(2m+1)}{r_y} \right\}$. Solutions for Eq. 3.20 are

$$k = \gamma \pm \sqrt{\gamma^2 + \beta_l^2} \tag{3.21}$$

Note that $\gamma \sim \frac{1}{r_{x,y}}$ whereas $\beta_l \sim \frac{1}{h}$ (Eq. 3.5). From the cavity dimensions: $h \approx 1\mu m$, and width $\sim 20\mu m$, we may expect that $\gamma \ll \beta$. If we make this assumption, and keep in mind that $k > 0$, Eq. 3.21 becomes

$$k = \gamma + \beta_l \left(1 + \frac{1}{2}\frac{\gamma^2}{\beta_l^2} + ...\right) = \beta_l \left(1 + \frac{\gamma}{\beta_l} + \frac{1}{2}\frac{\gamma^2}{\beta_l^2} + ...\right) \tag{3.22}$$

so that

$$\lambda = \frac{2\pi}{k} = \frac{2\pi}{\beta_l} \left(\frac{1}{1 + \frac{\gamma}{\beta_l} + \frac{1}{2}\frac{\gamma^2}{\beta_l^2} + ...}\right) \approx \frac{2h}{l}\left(1 - \frac{\gamma}{\beta_l}\right). \tag{3.23}$$

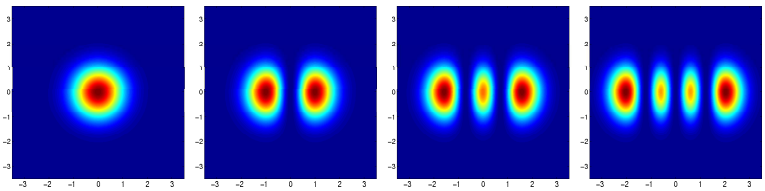

(a) $\psi_{[00]}$ (b) $\psi_{[10]}$ (c) $\psi_{[20]}$ (d) $\psi_{[30]}$

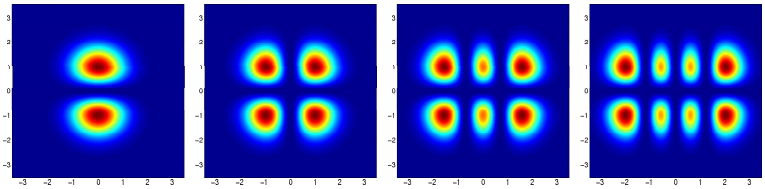

(e) $\psi_{[01]}$ (f) $\psi_{[11]}$ (g) $\psi_{[21]}$ (h) $\psi_{[31]}$

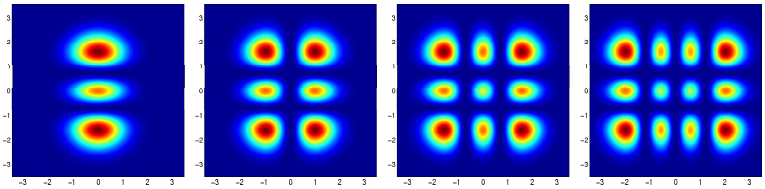

(i) $\psi_{[02]}$ (j) $\psi_{[12]}$ (k) $\psi_{[22]}$ (l) $\psi_{[32]}$

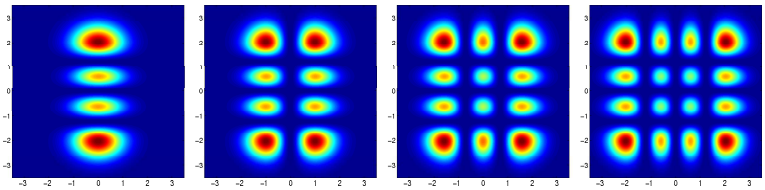

(m) $\psi_{[03]}$ (n) $\psi_{[13]}$ (o) $\psi_{[23]}$ (p) $\psi_{[33]}$

Figure 3.1: Examples of Hermite Gaussians $\psi_{[nm]}(x,y) = H_n\left(\frac{\sqrt{2}x}{w_x}\right) H_m\left(\frac{\sqrt{2}y}{w_y}\right) e^{-\left(\frac{x^2}{w_x^2}+\frac{y^2}{w_y^2}\right)}$, the x- and y- dependent part of the solutions to the wave equation Eq. 3.3 ($E(\mathbf{r}) = \psi(x,y)sin\left(\frac{l\pi}{h}z\right)$). Here $w_x = w_y = 1/\sqrt{2}$

Substituting back 2γ and realizing that the *wavelength in vacuum* $\lambda_0 = n_0\lambda$, we end up with

$$\lambda_{[nml],0} = n_0 \left(\frac{2h}{l} - \frac{h^2}{\pi l^2} \left\{ \frac{(2n+1)}{r_x} + \frac{(2m+1)}{r_y} \right\} \right) \tag{3.24}$$

for the wavelength that we would detect. The label $[nml], 0$ indicates the mode numbers of the $x-, y-$, and $z-$component and the 0 indicates that this is the wavelength in vacuum. In the following we will skip the l and 0 in the labeling, keeping in mind that the wavelengths are in vacuum and, as we will see, for a certain value of l. Written more conveniently equation 3.24 becomes

$$\lambda_{[nm]} = \lambda_{[00]} - an - bm \tag{3.25}$$

with

$$a = \left(\frac{2n_0 h^2}{\pi r_x l^2} \right) \tag{3.26}$$

$$b = \left(\frac{2n_0 h^2}{\pi r_y l^2} \right) \tag{3.27}$$

$$\lambda_{[00]} = \frac{2n_0 h}{l} - \left(\frac{a+b}{2} \right) \tag{3.28}$$

3.2 Anisotropy

At this point we realize that we have assumed the refractive index to be isotropic, i.e. not dependent of the polarization of the light. We can make our model a little bit more general if we replace $k_0^2 n^2(\mathbf{r})$ by the tensor

$$\epsilon = \begin{pmatrix} \epsilon_{xx} & 0 \\ 0 & \epsilon_{yy} \end{pmatrix} \tag{3.29}$$

with

$$\epsilon_{xx}(x,y) = \epsilon_m \left(1 - \frac{x^2}{r_{xX}^2} - \frac{y^2}{r_{yX}^2} \right) \tag{3.30}$$

$$\epsilon_{yy}(x,y) = \epsilon_m \left(1 - \frac{x^2}{r_{xY}^2} - \frac{y^2}{r_{yY}^2} \right). \tag{3.31}$$

X and Y indicate different polarization. Note that we only consider polarizations in the x- and y-direction. If r_{xX}, r_{yX}, r_{xY} and r_{yY} all differ a little bit, then in analogy of the earlier derivation, this would induce a spectrum like

$$\lambda_{[nm]X} = \lambda_{[00]X} - a_X n - b_X m \tag{3.32}$$

$$\lambda_{[nm]Y} = \lambda_{[00]Y} - a_Y n - b_Y m. \tag{3.33}$$

We will use later these expressions for fitting experimental data (see section 5.1.2).

Chapter 4

Experimental setup

4.1 sample

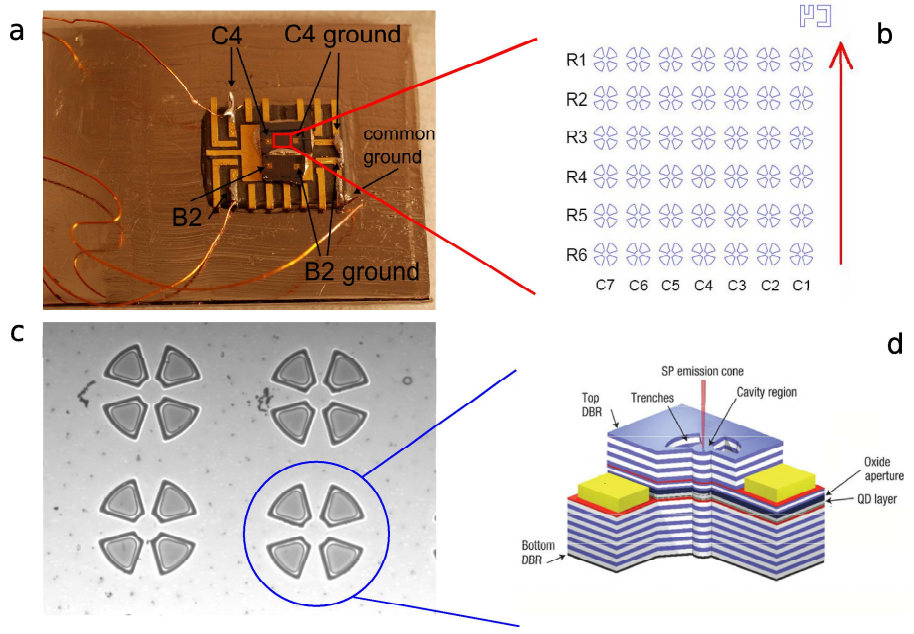

Figure 4.1: The sample is mounted on a sample holder (a). It consists of 6×7 cavities, labeled with row- and column- numbers (b). Four trenches are etched to make each cavity(c). Each cavity has a design equivalent to (d) (see section 4.1.1).

We study the C4 sample (See Fig. 4.1). It is mounted on a chip carrier. The sample contains 6×7 cavities. *We will refer to them by indicating the row and the column number* (for example R3C5). For a more detailed explanation of the design, see the section below.

4.1.1 Cavity design

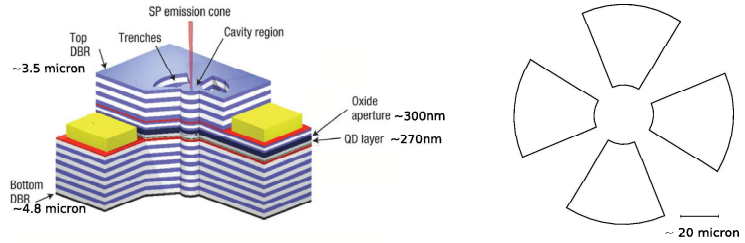

Figure 4.2: The cavity has two DBRs (distributed Bragg mirror): the bottom DBR has 32 layers, and the top DBR has 23 layers. In between these DBRs there is an oxide aperture and an active region with a quantum dot layer. The trenches are formed by optical lithography and reactive-ion etching and penetrate up to ten bottom mirror layers[5]. The diameter of the cavity is about 30 μm.

The sample design is shown in Fig. 4.2. The following information is from a file giving specifications on this sample (see [4]), and the knowledge of Dapeng Ding.

The cavities have been etched in a crystalline structure which consists of two DBRs with a quantum dot layer and an oxide aperture in between them. The bottom DBR has 32 layers, whereas the top DBR has 23, in order to guide the emission to the top. They are both made of alternating GaAs and Al0.9Ga0.1As. The total thickness of the bottom and the top DBR are respectively 4.8 μm and 3.5 μm.

The active region consists of GaAs and contains a self-assembled quantum dot layer of InGaAs grown by molecular beam epitaxy. The oxide aperture area consists of layers of $Al_{0.75}Ga_{0.25}As$, AlAs, $Al_{0.83}GaAs$ and $Al_{0.75}GaAs$. The active region is about 270 nm and the oxide aperture is 300 nm.

The trenches are formed by optical lithography and reactive-ion etching and penetrate up to ten bottom mirror layers[5]. This defines the oxidation front: after etching the trenches, oxide is added to form the oxide aperture. After oxidation the AlAs layer is partially transformed into AlxOy, creating an aperture about 2 μm in diameter. The diameter of the cavity is about 30 μm.

4.2 Cryostat

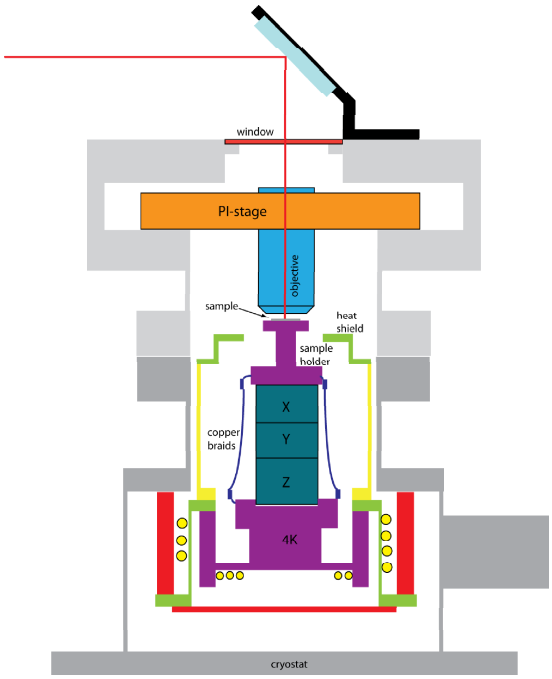

Figure 4.3: The sample is mounted on a sample holder, which is mounted on attocubes. The attocubes allow us to move the sample in the x- y- z-. A microscope objective is mounted in a PI-stage, which we can control with a computer and which enables us to move the objective in the x- and y- direction.

As we can see in Fig. 4.3, the sample is mounted on a sample holder in a cryostat. This holder is mounted on attocubes. Attocubes are able move in the x- y- z- direction with a precision better then 0.1 μm. We use them to move the sample to a cavity of interest.

To focus the excitation laser on the sample and the collect the emission from the sample, we use two different optical elements (each for other experiments):

- Microscope objective: 80× magnification, N.A. 0.9, focal length 2.5 mm, working distance 0.3 mm
- Aspheric lens: N.A. 0.6, focal length 4.02 mm

Note: Because we mainly use the microscope objective, I will use the word 'objective' in this thesis to explain experiments. Only if we use the aspheric lens I will make an explicitly note this. The objective is mounted in a PI-stage, which enables us to move the objective with a precision of 0.1 nm (according

to the company), which is good enough, for we need a resolution of o.1 μm. We are able to *control* the PI-stage with a computer to spatially scan the cavity.

It should be mentioned here that we perform all our measurements at vacuum (4.6×10^{-6} mbar).

4.3 Optical path

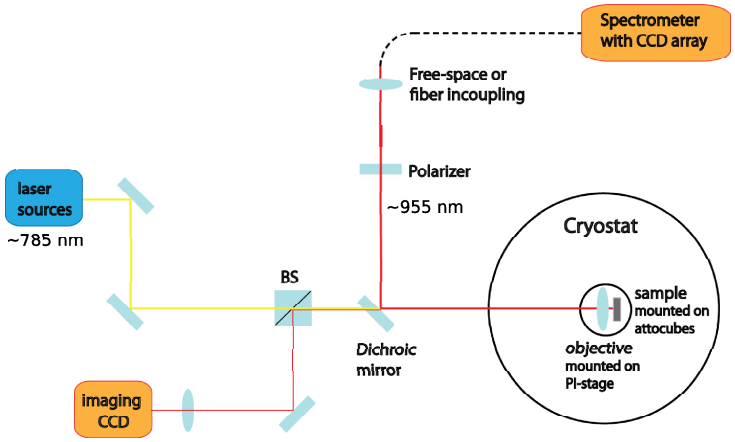

Figure 4.4: Optical path. During the experiments we vary the polarizer, the path to spectrometer and the laser source.

The optical path is shown in Fig. 4.4. We excite the cavities with laser light of wavelength 785 nm, which is well above (the energy of the photons) the band gap of GaAs. On the way to the sample the laser beam goes through a beam splitter, a dichroic mirror (R 920 nm T 780 nm) and through the objective. The ligth, reflected from the sample, goes back through the dichroic mirror and is partly reflected to go to a CCD-camera. With this camera we can see the surface of the sample when the sample is moved out of the focus. Because of excitation by the laser, electron hole pairs are created. The recombinations act as an internal light source of different wavelengths. Thus also the cavity modes with wavelengths 955 nm come out of the sample. They are reflected by the dichroic mirror. On their way to the *spectrometer* they may pass a polarizer and couple into free space, a multi-mode fiber or a single mode fiber.

During the experiments we vary certain optical elements:

- Laser sources:
  - Diode laser: 785 nm power in the order of mW
  - Titanium-Sapphire Ring laser: 770 nm power same order of magnitude
- Polarizers:

  - No polarizer
  - Glan-Taylor on a rotation stage rotated by hand
  - Linear film polarizer on motorized rotation stage
  - $\lambda/2$-plate on motorized rotation stage in front of a fixed linear film polarizer

- incoupling to spectrometer:
  - Free space
  - Multi-mode fiber
  - Single-mode fiber

- To focus the beam on the sample:
  - Microscope objective: 80× magnification, N.A. 0.9, focal length 2.5 mm, working distance 0.3 mm, and
  - Aspheric lens: N.A. 0.6, focal length 4.02 mm.

When the experiments are explained I will always make reference to these elements. Note that only the microscope objective is used, unless explicitly mentioned.

4.3.1 Spectrometer

We use a spectrometer based on a grating. There are a few things that are important to note about the spectrometer.

Spectra What comes out of the spectrometer are spectra: every specified time interval (in many cases 1 s) a CCD-camera is read out per pixel (1024 in total). Each pixel corresponds to a certain spectral range. We end up with an array of 1024 elements containing the counts per time interval. With a calibration lamp we can calibrate the spectrometer, so that we know the wavelengths. Nevertheless, in this thesis I will sometimes refer to the pixel numbers.

Calibration Note here: we have only once performed a calibration. This gave us the formula for the wavelength $\lambda = 0.016363 * (pixelnumber) + 952.21$, when the spectrometer is positioned at 953 nm. The range of a spectrum is thus 16,75 nm, which corresponds to 1024 pixels.

Resolution The resolution of the spectrometer is higher then the cavities. By this we mean that the line width observed when measuring a narrow bandwidth light source, such as a laser or a calibration lamp, is smaller than spectral peaks from the cavity. The formula for wavelengths also gives an idea of how precisely we can be can determine wavelengths from a given spectrum. One pixel shows a band width of 0.0164 nm. I assume that the pixels of the spectrometer are chosen such that they do not go beyond the 'resolution of the grating'. With fitting a Gaussian to a peak I can reach an accuracy better than half a pixel. From this I conclude that from a spectrum we know the wavelengths up till two decimal behind the comma.

Polarization dependence During the measurements it became clear that the spectrometer is sensitive to the polarization of incoming light (See also section 5.1.2). This is due to the grating within the spectrometer. It is well known that grating have a polarization dependent diffraction efficiency.

Chapter 5

Results

With our setup we can perform measurements on spectra, either polarization resolved or not, and spatial scans.

5.1 Spectra

In the following we will look at the spectra of some cavities, either polarization resolved or not. Also we will try to find a way to describe them by trying to fit models to the data. I use Matlab to depict the data and to make fits (Appendix B).

5.1.1 Not polarization resolved

Figs. 5.1(a) and 5.1(b) show respectively the spectra from the R1C1- and the R1C4-cavity, both obtained with the multi-mode fiber path and the diode laser as pump. Please note here that the noise increases as you go from long to shorter wavelengths. This is typical for measuring with a multi-mode fiber.

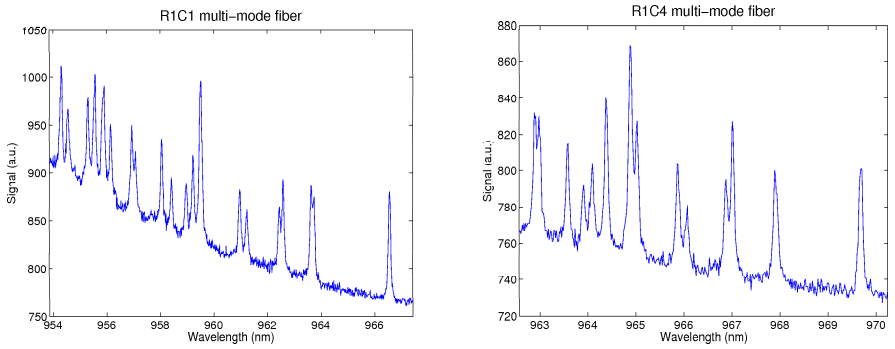

(a) R1C1-cavity

(b) R1C4-cavity

Figure 5.1: Spectra of the R1C1 and R1C4 cavities taken without polarizer. We used the multi-mode fiber to couple in to the spectrometer.

One can observe that going from long to shorter wavelengths the number of peaks increases. Most peaks are split into two or rather *appear in pairs*. At first glance let us assume that the peaks of such a pair are related. We will now look at *centers of pairs*, by which we mean the wavelength right in between the two wavelengths of two peaks. As we will show, for both cavities the centers satisfy quite accurately the *empirical* model

$$\lambda_{[nm]} = \lambda_{[00]} - an - bm, \tag{5.1}$$

with $n, m = 0, 1, 2, ...$ and $\lambda_{[00]}$ the wavelength of the peak on the right end of the spectrum. With this model we can provide the pairs with labels $[nm]$ so that its wavelength $\lambda_{[nm]}$ is given by Eq. 5.1. We always always label the peaks such that $a > b$ and thus $\lambda_{[10]} > \lambda_{[01]} > \lambda_{[00]}$. Once we have provided the pairs with labels, we can perform a least squares fit to optimize the parameters a, b, and $\lambda_{[00]}$ (see Appendix B!).

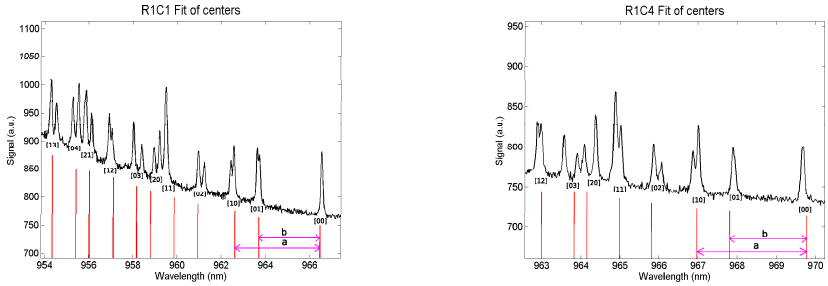

(a) R1C1 (b) R1C4

Figure 5.2: With the empirical model $\lambda_{[nm]} = \lambda_{[00]} - an - bm$ we provide pairs of R1C1 and R1C4 with labels $[nm]$. The red lines show a least square fit which optimizes a, b, and $\lambda_{[00]}$. Note: the height of the red lines is *chosen* to follow the noise level. It has *no physical meaning*. Table 5.1.1 shows the fit parameters.

In Fig. 5.2 the pair of R1C1 and R1C4 are labeled. The red lines show least squares fits to their centers. Note that the height of the red lines is chosen just to follow the noise level. Be not tempted to address a physical meaning to them. Table 5.1.1 shows the fit and goodness parameters of these fits. From these parameters we could qualitatively say that for R1C1, Eq. 5.1 predicts most wavelengths of the centers with an accuracy of approximately 6% and the maximal error lies within 14%. For the R1C4 cavity these numbers are 4% respectively 7%. Note that so far we have only looked at pairs of peaks. We will not yet discus about the separate peaks: the modes.

Table 5.1: Fit and Goodness parameters of least square fit to the pairs of the spectra from R1C1 and R1C4.

Cavity	Fit parameters			Goodness parameters			
	$\lambda_{[00]}$	a (nm)	b (nm)	RMSD (nm)	Emax (nm)	RMSD/b	Emax/b
R1C1	966.4788	3.8386	2.7633	0.1614	0.3689	0.0584	0.1335
R1C4	969.7882	2.8127	1.9878	0.0860	0.1543	0.0432	0.0776

5.1.2 Polarization resolved

Splitting

So far we have only looked at the spectra of R1C1 and R1C4, taken without polarizer. We found that the centers of pairs of peaks appear to be described quite accurately by Eq. 5.1.

We will again look at spectra of the R1C1 and the R1C4 cavity but this time with a polarizer (Glan-Taylor) placed in the path to the spectrometer. We use again the diode laser as a pump and multi-mode fiber incoupling (see section 4.3).

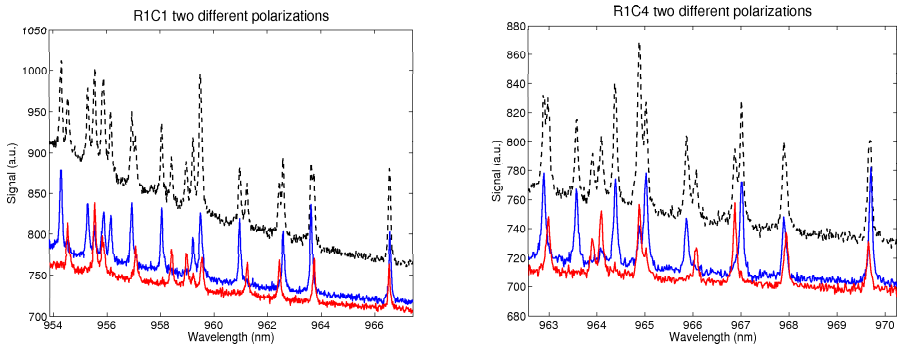

(a) R1C1 (b) R1C4

Figure 5.3: Spectra from the R1C1 and R1C4 cavities, taken with polarizer. The red an the blue lines show spectra for perpendicular positions of the polarizer. The dashed black line shows the spectra, taken without polarizer.

(See Fig. 5.3) In both Figs. 5.3(a) and 5.3(b) three line are depicted. In both figures the blue line shows a spectrum for a certain position of the polarizer, whereas the red shows the spectrum for the perpendicular position of the polarizer. The dashed black line shows again the spectrum that we obtained without polarizer.

From these results we can conclude that the two peaks within a pair have different polarization. This suggests further labeling. We already had labels $[nm]$, defining the mode number. Now we can also provide each peak with an X- and Y- label, which makes reference to its polarization. In Fig. 5.4 the dashed black line (the spectrum taken without polarizer)is provided with $[nm]$-, X- and Y-labels. Now it appears that also the peaks $\lambda_{[nm]X}$ and $\lambda_{[nm]Y}$ satisfy a rule like Eq. 5.1. This suggests a model for the wavelengths $\lambda_{[nm]X}$ and $\lambda_{[nm]Y}$ given by

$$\lambda_{[nm]X} = \lambda_{[00]X} - a_X n - b_X m \tag{5.2}$$
$$\lambda_{[nm]Y} = \lambda_{[00]Y} - a_Y n - b_Y m. \tag{5.3}$$

We will now try to fit this model to the data (see Appendix B). Fig. 5.4 shows the fits on the data of R1C1 and R1C4. The blue and the red vertical lines show the fit of the wavelengths to respectively the X- and Y- labeled

peaks. Again note: their heights is chosen to follow the noise level. They have no physical meaning. The fit parameters are given in Table 5.1.2.

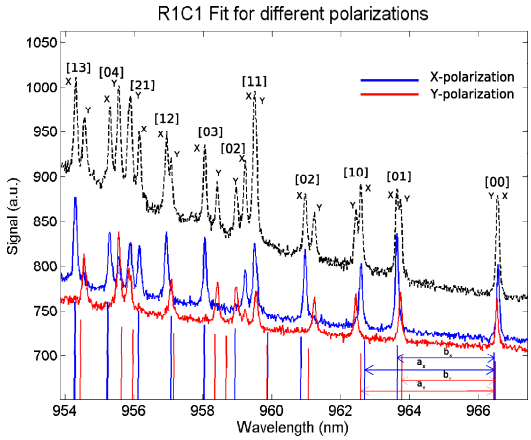

(a) R1C1

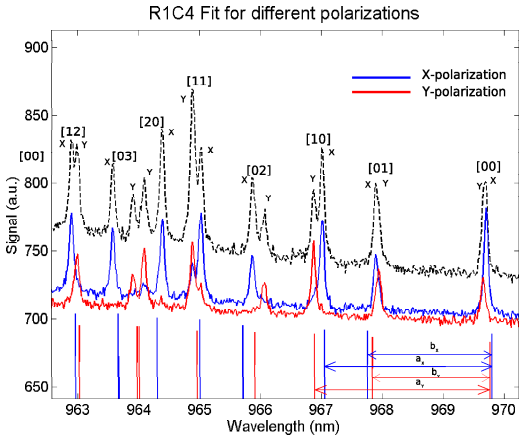

(b) R1C4

Figure 5.4: The blue and the red vertical lines show the fit of the wavelengths to respectively the X- and Y- labeled peaks.

What should be noted from Figs. 5.4(a) and 5.4(b) is that not only the positions of the peaks are described quite accurately, but also the splitting of two peaks within a pair. For example the peaks of the [11]-mode of R1C1 are separated by a small amount. The fit also shows a small splitting. Also for almost every pair the fit puts the X- and Y- polarization in the right order. If I had more time I would try to add numbers to the statements above. We can conclude that the model by Eqs. 5.2 and 5.3 gives a good description of the spectrum. From the theoretical model discussed in section 3.2 we may suggest that the splitting is due to anisotropy of the material (birefringence), for this model predicts the same spectrum. This model would predict two polarizations X and Y.

Table 5.2: Fit and Goodness parameters of least square fit of the model Eqs. 5.2 and 5.3 to the labeled peaks of R1C1 and R1C4.

Cavity	Fit parameters			Goodness parameters			
	$\lambda_{[00],X,Y}$	$a_{X,Y}$ (nm)	$b_{X,Y}$ (nm)	RMSD (nm)	Emax (nm)	RMSD/b	Emax/b
R1C1 X	966.4561	3.7642	2.8073	0.1616	0.3767	0.0576	0.1342
R1C1 Y	966.5014	3.9130	2.7194	0.1683	0.3611	0.0619	0.1328
R1C4 X	969.8102	2.7507	2.0463	0.0950	0.1430	0.0464	0.0699
R1C4 Y	969.7662	2.8746	1.9293	0.0838	0.1656	0.0434	0.0858

Polarization angles

Up to this point we are able to characterize modes by a mode number $[nm]$ and an X- or Y- label indicating its polarization. Interesting questions are now: can we describe the polarization angles of the modes? Do the modes fall apart into two polarizations? How is this polarization oriented relative to the trenches? To search an answer to these questions, we do the following experiment: place a polarizer in the path to the spectrometer. Take a spectrum for different settings of the polarizer separated by a specified step size. From these data we can make make a 2D plot: depict a spectrum for each polarization angle. Note that in the following the 'pixels' (of the 2D plot) are interpolated.

Fig. 5.5 shows a 2D plot of the results from a measurement on R1C1, using the Glan-Taylor polarizer and multi-mode fiber in coupling. The polarization range is 0 to 350 degrees and the step size is 10 degrees.

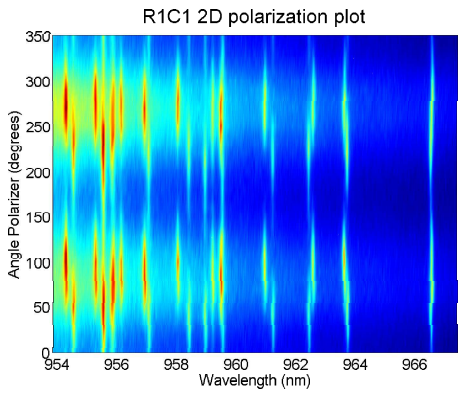

Figure 5.5: R1C1: 2D plot of spectra for different polarization angles. The polarization step size is 10 degrees.

In Fig. 5.5 we could search for polarization axes, but there is a problem. As mentioned before, the spectrometer is sensitive to polarization. We can clearly see that here, because not only the signal, but the background also changes with polarization. We could try to normalize these data. I will leave this to others because of a lack of time.

Fortunately, we have performed other experiments on another cavity: R5C6. We have made spatial scans (see section 5.2) for different polarizations. When we sum for every pixel number over all positions of a spatial scan, we end up

with a spectrum. We use these spectra to make the 2D plots. Fig. 5.6 show the results of two measurements on R5C6, using:

- The microscope objective and the linear film polarizer (Fig. 5.6(a)).
- The aspheric lens and the $\lambda/2$ plate in combination with the fixed polarizer (Fig. 5.6(b)).

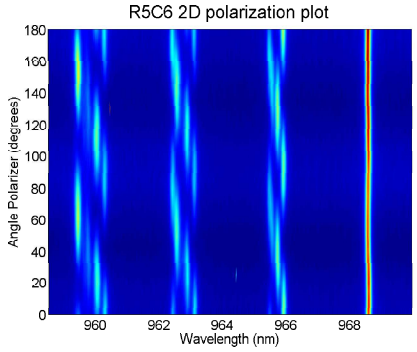

(a) $\lambda/2$ plate in combination with the fixed polarizer

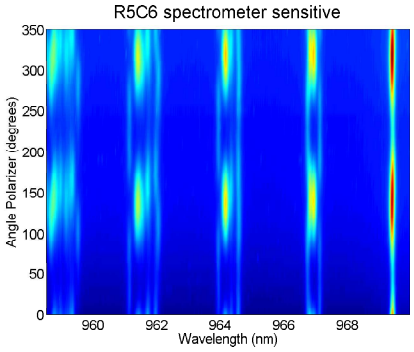

(b) Linear film polarizer

Figure 5.6: R5C6: 2D plot of results for spatial scans (see 5.2) for different polarizations. The spectra are obtained by summing for each pixel number over all positions of the spatial scan.

From Fig. 5.6 we can learn that the angles of polarization do not simply fall apart in two polarizations. It goes beyond the scope of this thesis to find a good description of the polarization of the modes. I can only speculate that the tensor as in Eq. 3.29 should contain non-zero elements ϵ_{xy} and ϵ_{yx}.

5.2 Spatial scan

5.2.1 Non polarization resolved

Until now we have only looked at spectra, either polarization resolved or not. Another experiment we can do, is what we call a spatial scan. To be short: we move the objective with the PI-stage to specified positions and take a spectrum at each position. Most essential in this experiment is that we use the *single-mode fiber* to couple into the spectrometer. The diameter of the single-mode fiber is about 5 μm. This enables us to image only a very small spot on the sample to the fiber.

To make a spatial scan, we first bring a cavity in a position, such that a clear spectrum is visible. We then specify a lattice of positions by giving the lower- and upper- boundaries and the step sizes in the x-positions and y-positions. A program controls the PI-stage, moving the objective to all specified positions, and takes a spectrum at each position.

In the following we will the following terms:

- **Spatial scan data** The set of data obtained from a spatial scan.
- **Spatial scan spectrum** When we sum for every pixel number over all positions of a spatial scan, we end up with a spectrum which we will call spatial scan spectrum.
- **Spatial image (at ... nm)** The image of the data at a specific pixel number (which corresponds to a certain wavelength) of the spatial scan data.

We have performed a spatial scan on R5C6 over an area of 10 μm × 10 μm with a step size of 0.1 μm. Fig. 5.7 shows spatial scan spectrum of R5C6. The peaks are provided with labels which refer to the spatial images in Fig. 5.9 at that specific wavelength.

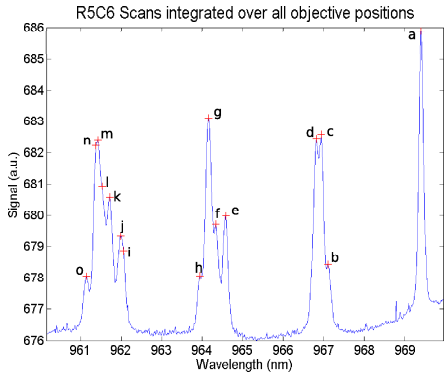

Figure 5.7: Spatial scan spectrum of R5C6. The peaks are provided with labels which refer to the spatial images in Fig. 5.9 at that specific wavelength.

In order to get a feeling of the size of the modes relative to the trenches, a blue square of (scaled) size 10 μm × 10 μm is depicted in Fig. 5.8. Also the purple lines show the x- and y- direction of the PI-stage (which is not perfectly aligned with the sample).

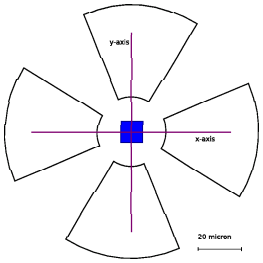

Figure 5.8: The scanned area (10μm x 10μm) depicted schematically in the cavity structure as well as the x- and y- direction of the PI-stage.

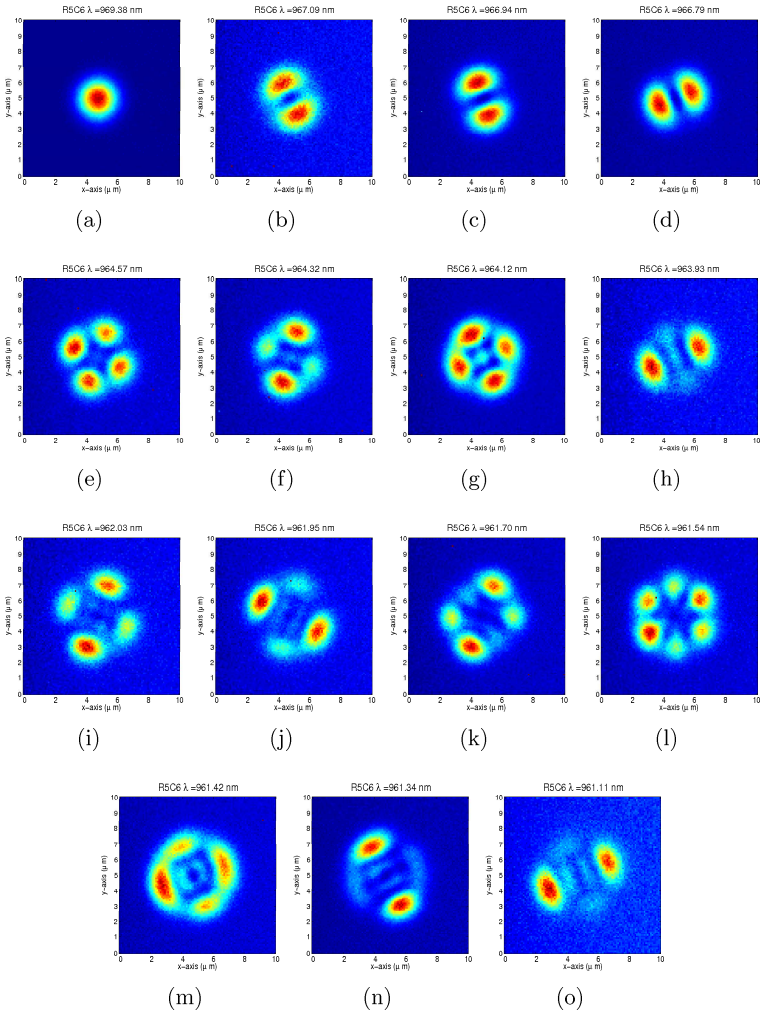

Figure 5.9: Results of a spatial scan on the R5C6. Each image shows the spatial image (10 μm × 10 μm) at the wavelength which is specified in the title. The labels and wavelengths correspond to the those in figure 5.7.

At first glance the images of Fig. 5.9 look like the Hermite-Gaussian plots in Fig. 3.1.

Let us consider the scan image of Fig. 5.9(c). It shows two blobs and looks like the [01] or the [10] modes in Fig. 3.1. (See Fig. 5.10) We will first have a look at values of the image along a line, which goes through the centers of the blobs(See Fig. 5.10(a)). Note that the line is constructed by specifying two points $(i_{1,2}, j_{1,2})$. I chose these points just by eye. In Fig. 5.10(b) these values are depicted by the purple dots. The red line shows a fit of $\left(H_1(x)e^{-\frac{x^2}{2}}\right)^2$ (of course provided with fit parameters) through these points.

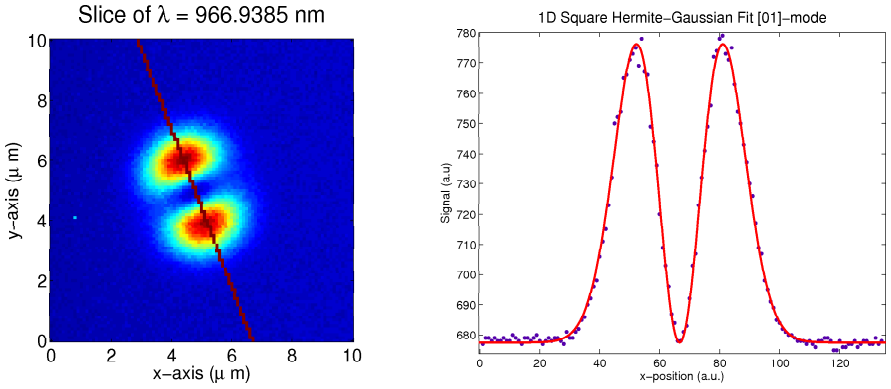

(a) (b)

Figure 5.10: Data of image from 5.9(c). The values along the red line in Fig. 5.10(a) are depicted in Fig. 5.10(b). The red line shows a fit of the square of the first order Hermite function to these values.

From this fit we can suspect that the image of Fig. 5.9(c) is well described by $\psi^2_{[01]}(x, y)$ (from Eq. 3.17). Let us find the fit parameters (see Appendix B.2) and use them to make a plot. The result is shown in Fig. 5.11.

This fit and the comparison of Fig. 5.9 with Fig. 3.1 indicates that the spatial modes are indeed described by Hermite Gaussians. It is beyond the scope of this thesis to go into more detail on this.

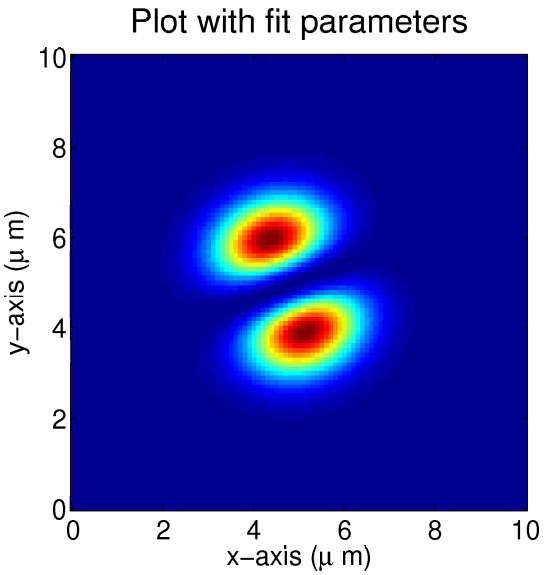

Figure 5.11: Plot of 2D fit of $\psi^2_{[01]}(x, y)$ (from Eq. 3.17) on the spatial image of Fig. 5.9(c).

Chapter 6

Conclusion and Outlook

In this thesis we have studied the optical modes of several micropillar cavities. We saw that with our setup we are able to analyze their spectra as well as the spatial structure of their modes. A simple model, which assumes quadratically decreasing refractive index and slight anisotropy, provides us with predictions on the spectra and the spatial structure of the modes. Results for the spectra an spatial modes are quite well described by these predictions, whereas the polarization of the modes is not. It is an intriguing question what sets these polarizations.

6.1 Outlook

It should as first be noted that this thesis shows only a part of the analysis that is performed on the cavities. For suggestions of more analysis, see Appendix C.

One of the motivations for finding a good description of the cavity modes is to make the fundamental mode ([00]) degenerate, which means that the peaks of the two polarizations lie on top of each other. This is needed for some quantum information schemes and algorithms. A way to do this (already shown by Cristian Bonato) is by burning holes next to the trenches.

It would be very challenging and interesting to try to find a better tensor ϵ to describe the material, and from that derive the optical modes of the cavities.

Chapter 7

Acknowledgements

Here I would like to thank some people for everything they have done. First I would like to thank Dirk Bouwmeester, who gave me the chance to work in his group. Then I would like to thank Jan Gudat, my direct supervisor. He has spent a lot of time on building the setup in which I could do the measurements. Also he has automated the setup, which made it possible to perform the spatial scans. I would also like to thank Dapeng Ding and Christian Bonato, who were in our group as well. I could always ask them for advise, and they were always willing to help patiently. Next, I want to thank Evan Jeffrey, who made great contribution to this work by providing answers to all questions on Matlab. At last I want to thank Martin van Exter, who actually came up with the theoretical model for the refractive index, and provided me with literature on it. Also he helped me with questions on the writing of the thesis.

Appendix A

Hermite polynomials

The first 5 Hermite polynomials are given by:

$$H_0(x) = 1 \tag{A.1}$$
$$H_1(x) = 2x \tag{A.2}$$
$$H_2(x) = 4x^2 - 2 \tag{A.3}$$
$$H_3(x) = 8x^3 - 12x \tag{A.4}$$
$$H_4(x) = 16x^4 - 48x^2 + 12 \tag{A.5}$$
$$H_5(x) = 32x^5 - 160x^3 + 120x \tag{A.6}$$

One can define Hermite functions

$$\psi_n(x) = \frac{1}{\sqrt{n!\,2^n\sqrt{\pi}}}\,\mathrm{e}^{-x^2/2}H_n(x). \tag{A.7}$$

These Hermite functions are normalized solutions to the differential equation

$$\psi_n''(x) + (2n + 1 - x^2)\psi_n(x) = 0. \tag{A.8}$$

In Fig. A.1 the first 6 Hermite functions are depicted.

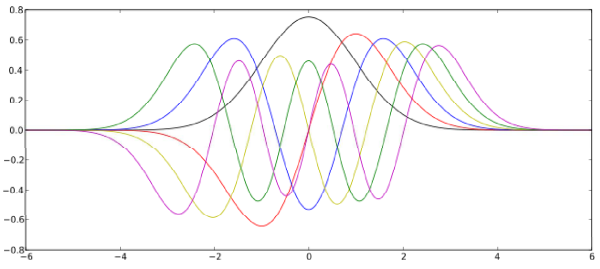

Figure A.1: Hermite functions (see Eq. A.7) 0 (black), 1 (red), 2 (blue), 3 (yellow), 4 (green), and 5 (magenta).

Appendix B

Matlab

B.1 Least square fitting $\lambda_{[nm]} = \lambda_{[00]} - an - bm$

Assume that we have a set of k labeled peaks and for each peak their wavelength $\lambda_{[nm],i}$. Then we have the set of equations

$$\left\{\lambda_{[nm],i} = \lambda_{[00]} - an_i - bm_i\right\}. \tag{B.1}$$

Define

$$A = \begin{pmatrix} 1 & a_1 & b_1 \\ 1 & a_2 & b_2 \\ & \vdots & \\ 1 & a_k & b_k \end{pmatrix} \tag{B.2}$$

Let $x = \left(\lambda_{[nm]},\ a,\ b\right)^T$ and $y = \left(\lambda_{[nm],1},\ \lambda_{[nm],2},\ ...,\ \lambda_{[nm],k}\right)^T$. Then $x^* = \left(\lambda^*_{[nm]},\ a^*,\ b^*\right)$ is said to be the least square solution of the equation

$$Ax = y, \tag{B.3}$$

if

$$|y^* - y| = |Ax^* - y| < |Ax - y| \quad \text{whenever} \quad x \neq x^*. \tag{B.4}$$

It is exactly this x^* that we calculate if we try to optimize $\lambda_{[nm]}$, a and b. Furthermore $y^* = Ax^* = \left(\lambda^*_{[nm],1},\ \lambda^*_{[nm],2},\ ...,\ \lambda^*_{[nm],k}\right)^T$ is the vector containing the wavelengths which *fit* best to the data (the vector y).

When we try to fit wavelengths to the formula $\lambda_{[nm]} = \lambda_{[00]} - an - bm$, we will call the elements in x^* the *optimized parameters* and the elements of y^* the *fit of the wavelengths*.

In order to get a feeling for the *goodness of a fit*, we can calculate now the following parameters: $RMSD$, $Emax$, $RMSD/b$ and $Emax/b$. The RMSD, the root mean square deviation (also called rms of the residuals), is defined as

$$RMSD = \left(\frac{1}{k} \sum_{i=1}^{k} \left(\lambda_{[nm],i} - \lambda^*_{[nm],i} \right)^2 \right)^{\frac{1}{2}}. \tag{B.5}$$

Intuitively one could see the RMSD as the average error. Emax is given by $Emax - \max_i \left| \lambda_{[nm],i} - \lambda^*_{[nm],i} \right|$ and is the maximal error. We can divide RMSD and Emax by b ($b < a$) to get $RMSD/b$ and $Emax/b$ which are measures of how big the RMSD and Emax are in comparison with a and b.

B.1.1 Matlab script

Example of Matlab script:

```
function a=mrfitpar(x1,x2,y,cwl)

%Here the 'fitparx' is optimized for the equation X*fitparx=y (X is an n x 3
%matrix, and fitparx=[lambda_00 a b]. y contains the measured values
X = [ones(size(x1))  x1  x2];
fitparpx = X\y;
Ypx = X*fitparpx;


%From here fit parameters are calculated:

%    # in pixel numbers
respx = Ypx-y;
RMDSpx = sqrt(mean(respx.^2));
Emaxpx = max(abs(respx));


%    # in nm
fitpar=fitparpxtowl(fitparpx,cwl)
RMDS=dispixtowl(RMDSpx)
Emax=dispixtowl(Emaxpx)

%    # dimensionless
dRMDS=RMDSpx/fitparpx(3)
dEmax=Emaxpx/fitparpx(3)
res=respx;

%A cell is created containing many fit parameters in

%   # pixel numbers
a{1,1}=fitparpx;
a{2,1}='optimized parameters pxn';
a{1,2}=Ypx;
a{2,2}='values given by the model pxn';
a{1,3}=RMDSpx;
a{2,3}='RMSD pxn';
```

```
a{1,4}=respx;
a{2,4}='residuals pxn';
a{1,5}=Emaxpx;
a{2,5}='Emaxpx';

%   #dimensionless
a{1,6}=dRMDS;
a{2,6}='RMSD/b';
a{1,7}=dEmax;
a{2,7}='Emax/b';

%   # nm
a{3,1}=fitpar;
a{4,1}='optimized parameters';
a{3,2}='not interesting';
a{4,2}='values given by the model';
a{3,3}=RMDS;
a{4,3}='RMSD';
a{3,4}=res;
a{4,4}='residuals';
a{3,5}=Emax;
a{4,5}='Emax';
```

B.2 2D Fitting

Assume you have a 2D-array A of data and you assume it to described by $f[a_1, a_2, ...](i, j)$ where $a_1, a_2, ...$ are parameters and i, j indicate the array coördinates. What we want is to optimize the parameters. One way is to find the minimum of

$$\chi^2(a_1, a_1, ...) = \sum_{i,j} \left(A_{ij} - f[a_1, a_2, ...](i, j)\right)^2 \tag{B.6}$$

for the parameters $a_1, a_2, ...$. This can be done using the lsqnonlin function in Matlab. Here you need to define a function $F(a_1, a_2, ...) = [f_1((a_1, a_2, ...)), f_1((a_1, a_2, ...)), ...]$, where for example $f_1(a_1, a_2, ...) = A_{11} - f[a_1, a_2, ...](1, 1)$. With the lsqnonlin function than tries to find parameters for which the length of $F(a_1, a_{2,...})$ is minimal (for more details, reed the manual of Matlab). The function can return the optimized parameters as well as parameters about the goodness of the fit.

B.2.1 Matlab script

Here is an example of function is shown.

```
function a = functofit2(SC,x);

%This script will define the function that should be fitted to some
%2D-array SC.
```

```
[n,m]=size(SC);
k=1;
%a = zeros(n*m, 1);

for i=1:n
    for j=1:m
        % for simplicity, we use p=(i-x(5)) and q=(j-x(6))
        xp= (  (i-x(5)) * cos(x(7)*2*pi/360) +  (j-x(6)) * sin(x(7)*2*pi/360)  )/x(3) ;
        yp= (  (j-x(6)) * cos(x(7)*2*pi/360) -  (i-x(5)) * sin(x(7)*2*pi/360)  )/x(4) ;
        a (k) =(  x(1) + x(2)* ( 2*(sqrt(2)*xp) * exp(  -xp^2  -yp^2 )  )^2  ) -SC(i,j) ;
        k=k+1;
    end
end
```

To make it an function only dependent of x (the fit parameters) use the following syntax:

```
@(x)functofit2(M{3,3},x)
\begin{thebibliography}{99}
```

Appendix C

Suggestions on futher analyzing

While doing the experiments mentioned in this thesis I have developed a lot of scripts in Matlab, which can enables one to analyze quickly data from measurements on the cavities (see Appendix B). Here I will make suggestions on interesting analysis that yet would be nice to perform. I have already seen nice features, but I was not able to put this in the thesis:

- Identify modes of R5C6
  - Use polarization resolved polarization scan to identify the modes for the zeroth, first and second order. The third order is more difficult.
  - For the modes second order modes try to fit superpositions:
    * $\left(\psi_{[nm]} + \psi_{[n'm']}\right)^2$
    * $\left(\psi_{[nm]} e^{i\phi} + \psi_{[n'm']}\right)^2$
    * $\left(\psi_{[nm]}\right)^2 + \left(\psi_{[n'm']}\right)^2$
  - Use the spatial scan of 20090526 and the polarization resolved spatial scan of 200905287
- Identify the modes of R3C4
  - compare $\frac{a}{b}$ with $\frac{w_y^2}{w_x^2}$

Bibliography

[1] Kerry J. Vahala, Optical microcavities, *Nature*, **424**, 839-846 (2003).

[2] Amnon Yariv, *Quantum Electronics third edition*, John Willey & Sons p. 640, 641.

[3] U. Rössler, D. Strauch, *Landelt Börnstein substance / Property index vol III / 41A1b*

[4] `http://www.physics.ucsb.edu/~susanna/jansample_feb24/` , filename: NIPQD.xls, 2009/03/30.

[5] Florian Haupt, *Fiber coupling of Quantum Dots in Micropillar Cavities*,Master Thesis ETHZ, Ferbruary 2009.